IOPscience iopscience.iop.org

Home Search Collections Journals About Contact us My IOPscience

Rotational branch analysis of the excitation of the fundamental vibrational modes of CO_2 by slow electron collisions

This article has been downloaded from IOPscience. Please scroll down to see the full text article.

1986 J. Phys. B: At. Mol. Phys. 19 1377

(http://iopscience.iop.org/0022-3700/19/9/018)

View the table of contents for this issue, or go to the journal homepage for more

Download details:
IP Address: 203.230.125.100
The article was downloaded on 23/06/2011 at 09:49

Please note that terms and conditions apply.

J. Phys. B: At. Mol. Phys. **19** (1986) 1377-1396. Printed in Great Britain

Rotational branch analysis of the excitation of the fundamental vibrational modes of CO_2 by slow electron collisions

Th Antoni†, K Jung, H Ehrhardt and E S Chang‡

Fachbereich Physik, Universität Kaiserslautern, D 6750, Kaiserslautern, West Germany

Received 22 July 1985

Abstract. At 2 eV, the simultaneous rotational-vibrational cross sections for the fundamental modes are found to be well described by the Born formula with just long-range interactions. However, this result is not obtained for pure vibrational excitation (Q branch) in the Raman-active Fermi diads. At 3.8 eV, the infrared-active ν_2 and ν_3 cross sections agree with a previous theory incorporating resonant and direct scattering coherently. Measurements on the Raman-active ν_1 mode indicate that theories need to account for the Fermi resonance.

1. Introduction

Recent reviews on electron-molecule collisions (Lane 1980, Trajmar and Cartwright 1983, Takayanagi 1984) have documented their many applications as well as the intrinsic interests. Of particular importance is the CO_2 high-power laser, where knowledge of ro-vibrational cross sections is essential to optimise the output of the laser system. The carbon dioxide molecule also possesses several attractive features for the purpose of this investigation. Its fundamental modes consist of a Raman-active (ν_1) and two infrared-active modes, ν_2 of Π and ν_3 of Σ symmetries. The relatively high position of the negative ion resonance at 3.8 eV extends the non-resonant (direct) scattering region up to 2 eV, where the requisite high electron energy resolution is easily maintained. Thus, the study of electron impact on CO_2 simultaneously explores the excitation of Raman-active as well as infrared-active modes, in both direct and resonant scattering. Especially with the resolution of rotational branches, such an investigation can be expected to selectively disclose the different excitation mechanisms—direct or resonant, long-range dipole, quadrupole and polarisability potentials, or short-range interactions and their interplay.

Earlier low-energy beam experiments have demonstrated that the differential cross sections (DCS) of the infrared-active vibrational modes have strong forward peaks in contrast to those of Raman-active modes (Andrick *et al* 1969). More detailed measurements of vibrational excitation in CO_2 have been made from 1 to 19 eV (Danner 1970) and from the resonance energy of 4 to 50 eV (Register *et al* 1980) with higher resolution. In the latter work, even with an energy resolution of 23 meV (FWHM), it was necessary to unfold the data just to separate out certain vibrational cross sections. Recently

† Present address: Jet Propulsion Laboratory, California Institute of Technology, 4800 Oak Grove Drive, Pasadena, CA 91109, USA.

‡ Department of Physics and Astronomy, University of Massachusetts, Amherst, MA 01003, USA.

0022-3700/86/091377+20$02.50 © 1986 The Institute of Physics

Kochem *et al* (1985a) have investigated the threshold behaviour of the excitation cross section for the three fundamental vibrational modes.

Theoretically, Itikawa (1971) has accounted for the low-energy infrared-active DCS by the dipole approximation up to $\theta = 20°$ by normalising the experimental data of Andrick *et al* (1969) to theory at 10°. More elaborate calculations are usually first performed in an adiabatic nuclei approximation (Morrison *et al* 1977, Morrison and Lane 1977). Then in the adiabatic-nuclear-vibration approximation, Morrison and Lane (1979) and Whitten and Lane (1982) have calculated the integrated vibrational cross sections in the threshold region.

Recent advances in experimental techniques have enabled us to achieve an energy resolution of about 10 meV and to successfully unfold rotational branch structure in CO (Jung *et al* 1982, Chang *et al* 1984). Since the rotational constant in CO_2 is five times smaller than in N_2 and in CO, deconvolution of the measured energy loss profiles may not be unambiguous without theoretical input. This is especially true when the separation between two vibrational modes is comparable with the energy resolution.

In this paper we report on the measurement of ro-vibrational cross sections in CO_2 at the resonance energy of 3.8 eV and below the resonance at 2 eV. In order to enhance the rotational effects, we have raised the gas temperature to 500 K resulting in an average rotational quantum number of $j = 20$. However, this increases the population of the first vibrational level to 22%. These hot-band contributions to excitation cross sections are considered here by generalising the theory for ro-vibrational excitation (Chang 1984). Further complications caused by the Fermi resonance not explicitly dealt with in the theory may render our analysis of the Fermi diads less accurate than the infrared-active modes.

2. Experimental procedure

The crossed-beam electron spectrometer used for the present study has already been described earlier (Jung *et al* 1982). Now the spectrometer is equipped with a differentially pumped gas beam and an additional cryopump in the vacuum chamber. The improved vacuum system results in a significant reduction of the background pressure to about 10^{-6} Torr when the gas beam is in operation. Together with the use of a thoriated iridium filament (0.1 mm diameter) instead of a tungsten one, drift effects in the electron optics during data acquisition are further reduced. For the present work, the energy resolution ranges between 11 and 13 meV, with a primary electron beam current of 10^{-10} A.

As in our previous work, absolute cross sections are determined from the relative flow method (Srivastava *et al* 1975). The required noble gas cross sections are taken from Andrick and Bitsch (1975).

3. Fundamental vibrational modes and theory for their excitation

The fundamental modes of CO_2, their vibronic symmetries and their energies are listed in table 1. For brevity, we refer to the ground state (000) as $v = 0$, the bending mode (010) as $v = 2$ (for ν_2) and the asymmetric stretching mode (001) as $v = 3$ (for ν_3). Nominally there is only one fundamental Raman mode, the (100) of Σ_g symmetry. However its energy coincides with that of the (020) overtone, resulting in strong mixing referred to as the Fermi resonance. Conventionally the upper level is designated (100)

Table 1. Properties of the fundamental modes.

	Mode	v	Symmetry	E (meV)	D_v (ea_0)	α_v (a_0^3)	α'_v $(a_0)^3$	q_v (ea_0^2)
Infrared	001	3	Σ_u^+	291	0.128[a]			
	010	2	Π_u	83	0.0713[b]			
Raman	upper	1	Σ_g^+	172		0.396	0.342	
	100 experiment[c]					0.505	0.448	
	theory[d]					0.96	0.705	−0.635
	lower	4	Σ_g^+	159		0.321	0.293	
	02^00 experiment[c]					−0.072	−0.078	

[a] Weighted average 0.1274 (Devi *et al* 1984) and 0.1296 (Rothman and Young 1981).
[b] Rothman and Young (1981).
[c] Akhmedzhanov *et al* (1982).
[d] Whitten and Lane (1982).

and the lower one (020). Actual calculations show that while the above convention holds for the carbon isotope $^{13}C^{16}O_2$, the composition of the normal species $^{12}C^{16}O_2$ is actually 46% (100) and 54% (020) for the upper level (Howard-Lock and Stoicheff 1971). Nevertheless we will continue to call the upper level $v=1$ (for ν_1), and will propose that the lower level be labelled $v=4$ (see table 1). At midway, the (02^20) state is found to be negligibly excited (see figure 13(c)).

A theory for ro-vibrational excitation by electron impact has been given by Chang (1984). A summary is given below to facilitate the discussion of results. Note that symmetry considerations restrict rotational transitions to Δj = even for $\Sigma_g \to \Sigma_g$ transitions (excitation of $v=1, 4$) and to Δj = odd for $\Sigma_g \to \Sigma_u$ transitions (excitation of $v=3$).

3.1. The infrared-active modes

Below the resonance region, vibrational excitation for the infrared-active modes in CO and in C_2H_2 has been found to be well described by the Born dipole approximation (Sohn *et al* 1985, Kochem *et al* 1985b). Following Takayanagi (1966), the rotational branch cross sections in CO_2 can be expected to be given by the Born formula,

$$d\sigma_v/d\Omega(j \to j') = A_j(4\tilde{k}D_v^2/3K^2). \tag{1}$$

In equation (1), A_j is the Hönl-London factor, and $\tilde{k}$ is the ratio of the final to the initial momenta of the electron. The square of the momentum transfer vector $\boldsymbol{K}$ is given by

$$K^2 = k^2(1+\tilde{k}^2-2\tilde{k}\cos\theta) \tag{2}$$

where k is the incident momentum in atomic units. In the case of CO_2, specific values of A_j for the ro-vibrational transitions are given in Chang (1984). From the sum rule, it can easily be seen that $A_j=1$ in (1) when rotational branches are summed. For convenience the vibrational transition moments D_v and the energies of the two fundamental infrared active modes are displayed in table 1.

In the region of the $^2\Pi_u$ resonance, the scattering is described by an approach using just a single partial wave in both the entrance and the exit channel (Chang 1984). For rotational transitions involving one unit of angular momentum transfer, an additional contribution comes from dipole scattering as described by (1) and its interference with

the resonance. Specifically for the ν_3 stretching mode, the Q branch ($\Delta j = 0$) vanishes, and the excitation cross section for the P and R branches ($\Delta j = \pm 1$) are given by (22) in Chang (1984). However, as will be seen in § 4, the $^2\Pi_u$ resonance does not excite the ν_3 mode appreciably. Therefore even at 3.8 eV, the rotational DCS are adequately given by (1).

In contrast, the $^2\Pi_u$ resonance can be expected to strongly excite the ν_2 bending mode (Andrick and Read 1971). Now state-to-state cross sections are constructed from table 2 and (19) and (20) of Chang (1984) and displayed below in the high-j approximation.

$$\frac{d\sigma_v}{d\Omega}(j\to j) = \frac{\tilde{k}}{2k^2}\left[N(\tfrac{5}{56}+\tfrac{3}{28}\cos^2\theta) + 2D_v\cos\chi\left(N\frac{(1+3\cos^2\theta)/30}{1+\tilde{k}^2-2\tilde{k}\cos\theta}\right)^{1/2} + \frac{4}{3}\frac{D_v^2}{1+\tilde{k}^2-2\tilde{k}\cos\theta}\right] \tag{3a}$$

$$\frac{d\sigma_v}{d\Omega}(j\to j+1) = \frac{\tilde{k}}{2k^2}\left[N(0.215-0.17\cos^2\theta) + \left(1-\frac{3}{2j}\right)D_v\cos\chi\left(N\frac{(1+3\cos^2\theta)/30}{1+\tilde{k}^2-2\tilde{k}\cos\theta}\right)^{1/2} + \frac{(j+2)}{(2j+1)}\frac{4}{3}\frac{D_v^2}{1+\tilde{k}^2-2\tilde{k}\cos\theta}\right] \tag{3b}$$

$$\frac{d\sigma_v}{d\Omega}(j\to j-1) = \frac{\tilde{k}}{2k^2}\left[N(0.195-0.124\cos^2\theta) + \left(1+\frac{3}{2j}\right)D_v\cos\chi\left(N\frac{(1+3\cos^2\theta)/30}{1+\tilde{k}^2-2\tilde{k}\cos\theta}\right)^{1/2} + \frac{(j-1)}{(2j+1)}\frac{4}{3}\frac{D_v^2}{1+\tilde{k}^2-2\tilde{k}\cos\theta}\right] \tag{3c}$$

$$\frac{d\sigma_v}{d\Omega}(j\to j+2) = \frac{\tilde{k}}{2k^2}N(0.249-0.157\cos^2\theta) \tag{3d}$$

$$\frac{d\sigma_v}{d\Omega}(j\to j-2) = \frac{\tilde{k}}{2k^2}N(0.233-0.165\cos^2\theta) \tag{3e}$$

$$\frac{d\sigma_v}{d\Omega}(j\to j\pm 3) = \frac{\tilde{k}}{2k^2}N(0.0402)\left(1\pm\frac{5}{2j}\right)(2+\cos^2\theta). \tag{3f}$$

Note that the cross sections for the transitions $j\to j\pm\Delta j$ are not proportional here as they were for $\Sigma\to\Sigma$ vibration excitations. For the sake of completeness the rotationally unresolved cross section is also given below.

$$\frac{d\sigma}{d\Omega}(v\to v') = \frac{\tilde{k}}{k^2}\left[\frac{N}{14}(8-3\cos^2\theta) + 2D_v\cos\chi\left(N\frac{(1+3\cos^2\theta)/30}{1+\tilde{k}^2-2\tilde{k}\cos\theta}\right)^{1/2} + \frac{4}{3}\frac{D_v^2}{1+\tilde{k}^2-2\tilde{k}\cos\theta}\right]. \tag{4}$$

Table 2. Integrated cross sections (10^{-16} cm^2).

Vibrational node	Δj (branch)		$E_0 = 2$ eV		$E_0 = 3.8$ eV
$\nu_1(100)$	0 (Q)		0.364[a]		0.59[a]
	+2 (S)		0.033[a]		0.22[a]
	−2 (O)		0.029[a]		0.19[a]
		sum	0.43	sum	1.0
$\nu_4(02^{\circ}0)$	0 (Q)		0.013[a]		0.3[a]
	+2 (S)		0.022[a]		0.21[a]
	−2 (O)		0.02[a]		0.19[a]
		sum	0.055	sum	0.7
sum $\nu_1 + \nu_4$			0.48 (0.5)		1.7 (1.73)
$\nu_2(010)$	0 (Q)		0.184		0.19
	+1 (R)		0.086		0.27
	−1 (P)		0.099		0.24
	+2 (S)		—		0.336
	−2 (O)		—		0.3
	+3		—		0.18
	−3		—		0.14
		sum	0.37 (0.48)	sum	1.66 (1.74)
$\nu_3(001)$	+1 (R)		0.43		0.28
	−1 (P)		0.41		0.26
		sum	0.84 (0.83)	sum	0.54 (0.49)

[a] Estimated by arbitrary extrapolation to 180° scattering angle.
Numbers in parentheses are derived from data of Danner (1970) for $E_0 = 2$ eV and $E_0 = 3.6$ eV impact energies.

3.2. The Raman modes

For non-resonant excitation of the Raman modes, the cross sections may also be evaluated in the Born approximation (Breig and Lin 1965). The Q branch is determined by the isotropic polarisability matrix element α_v,

$$d\sigma/d\Omega = \tilde{k}\alpha_v^2 K^2 N^2 \tag{5}$$

where

$$N = K^{-2}\int_0^{\infty} dr \sin KrC(r)/r^3 \tag{6}$$

The choice of the cut-off function $C(r)$ for CO_2 (Itikawa 1971) may affect the cross section by a factor of 2 or 3, rendering it difficult to compare theory with experiment. However, the ratio of cross sections for the Fermi diads should only depend on the ratio of α_v^2. For the Fermi diads, this ratio of the upper (ν_1) level at 172 meV to the lower (ν_4) level at 159 meV is known from Raman data to be 1.52 ± 0.02 (Howard-Lock and Stoicheff 1971). Thus our measurements of the Q-branch cross sections can provide a critical test of the Born theory.

In the case of the O($\Delta j = -2$) and S($\Delta j = +2$) branches, the cross sections are nearly isotropic and are given by

$$d\sigma_v/d\Omega(\Delta j = \pm 2) = B_j(\tilde{k}/5)(2Q_v/3 + \pi\alpha_v' K/16)^2 \tag{7}$$

where B_j is a squared Clebsch-Gordan coefficient given by Gerjuoy and Stein (1955). For $j = 20$, $B_j = 0.356$ and 0.393 for the O and the S branches respectively. In table 1 values for the quadrupole moment Q_v and the anisotropic polarisability α_v' matrix

elements are given along with the isotropic polarisability α_v. The experimental values are obtained from Raman scattering and depolarisation ratios, and then the deperturbed values are derived by disentangling the Fermi resonance (Akhmedzhanov *et al* 1982). These polarisability values are seen to be a factor of two lower than the theoretical values calculated from unperturbed states (Whitten and Lane 1982). In (6), the quadrupole term is dominant, but lacking an experimental value for Q_v we adopt the questionable theoretical value. For the purpose of an estimate the second term which is an order of magnitude smaller may be neglected, and the DCS is then isotropic.

In the resonance region, the Raman mode cross sections can be constructed from table 3 of Chang (1984). For example, the rotationally unresolved DCS is simply given for both Fermi diads by

$$d\sigma_v/d\Omega \propto 1+7\cos^2\theta. \tag{8}$$

However, this simple view is not in accord with experiment (Andrick and Read 1971). Therefore our data here are analysed without recourse to theory, and comparison is made with existing theories.

3.3. The 'hot-band' problem

We recall that in order to increase the rotational broadening of the energy loss profiles, we have raised the molecular beam temperature to 500 K. Consequently, 22% of the CO_2 molecules are in the first excited vibrational state (010). Thus measurements of the fundamental modes are contaminated by the nearby overtone modes known as 'hot bands' in infrared spectroscopy. For the infrared-active modes, hot-band effects can be determined from their known infrared intensities, and are found to be negligible. The situation is the simplest for the 001 mode and will be illustrated in § 4.1. Unfortunately, hot-band effects in the Raman modes are not known. Their neglect in the rotational branch analysis will result in larger uncertainties.

4. Results and discussions

To provide an overall picture of the observed modes, we show some energy loss spectra in figure 1. Direct excitation is most evident at a low incident energy and a small angle as in figure 1(*a*) ($E = 1.1$ eV and $\theta = 15°$). Besides the elastic peak, the only strong features are the fundamental infrared-active modes: ν_2 at 83 meV and ν_3 at 291 meV. Much weaker are the ν_2 superelastic peak, the Raman-active ν_1 mode at 172 meV and the overtone infrared-active mode at 461 meV.

At the resonant energy of 3.8 eV, the spectrum at 90° is quite different (figure 1(*b*)). While the ν_2 mode remains strong, the ν_3 mode has virtually disappeared. On the other hand, the ν_1 profile has become a dominant feature with the ν_4 mode appearing in the shoulder. In addition, combination and overtone modes involving ν_1 can also be seen. Detailed studies including rotational branches will be presented for the fundamental infrared-active modes in §§ 4.1 and 4.2, the Raman modes in § 4.3 and the integrated cross sections in § 4.4.

4.1. The asymmetric stretching mode, Σ_u (001)

The energy loss profiles have been measured at several low angles below 30° at both energies of 2.0 and 3.8 eV. They are all very similar and the ones at 10° are shown in

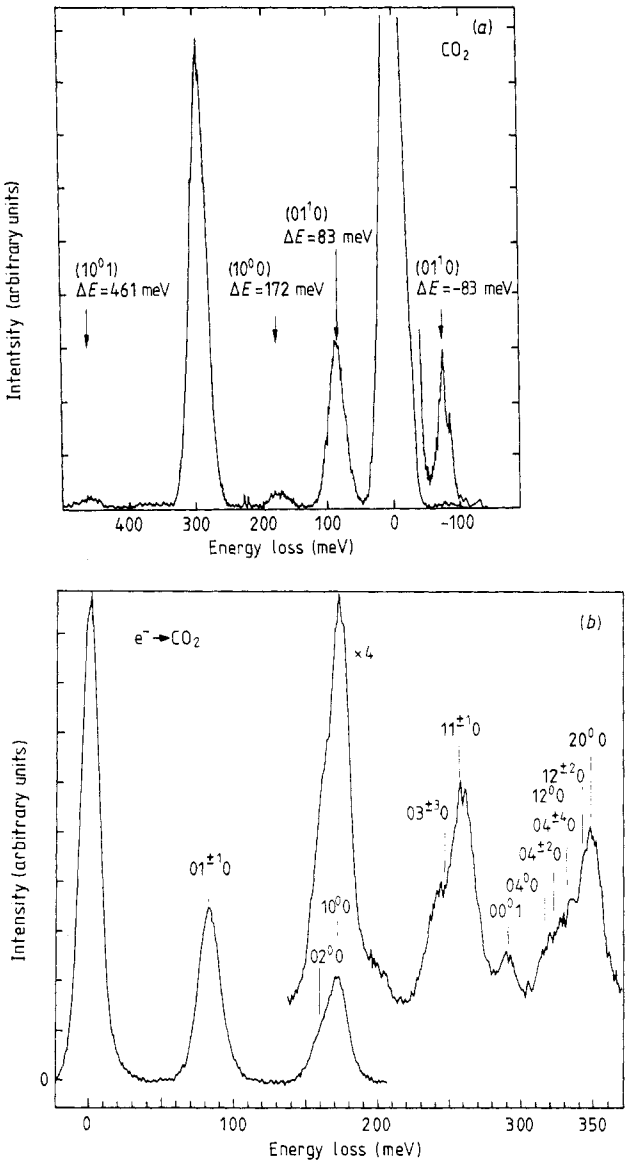

Figure 1. (*a*) Energy loss spectrum for an impact energy of $E_0 = 1.1$ eV and scattering angle $\theta = 15°$. Vibrational excitation is determined by direct electron-molecule interaction exclusively (from Danner 1970). (*b*) Energy loss spectrum for the impact energy $E_0 = 3.8$ eV, recorded at $\theta = 90°$. Vibrational excitation is dominated by resonance scattering.

figures 2(*a*) and 2(*b*) respectively. Also shown are the deconvoluted rotational branches, $P(\Delta j = -1)$ and $R(\Delta j = +1)$ with the assumed relative intensities given by the Hönl-London factors. The excellent fits at both energies show that the data are consistent with the Born theory given by (1). Beyond 30°, the DCS is too small for measurements with our high resolution of 12 meV.

To test the Born theory at larger angles, we resort to using the vibrational DCS of Danner (1970) and of Register *et al* (1980). When summed over all rotational branches, A_j in (1) becomes unity by a well known sum rule. The resulting expression is then

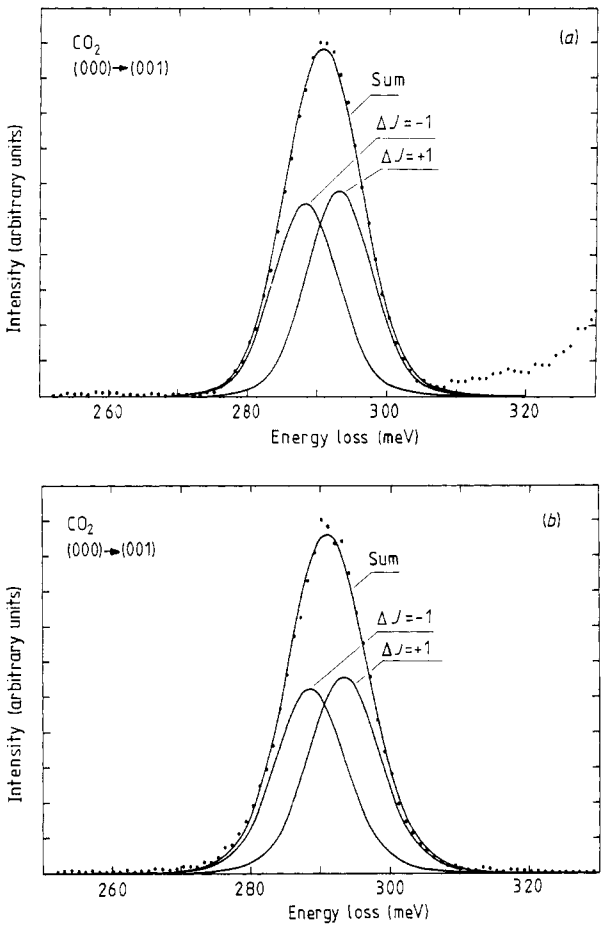

Figure 2. Energy loss profile for excitation of the asymmetric stretch mode, taken at $\theta = 10°$ for impact energies of 3.8 and 2 eV with an energy resolution of 12 meV. Lineshape analysis of these profiles requires inclusion of P and R branches only.

shown in figures 3(*a*) and 3(*b*) with the corresponding data at 2 and 3.8 eV respectively. Agreement between theory and experiment is very good at angles below 30° where the DCS are large and less so at the larger angles. Surprisingly the discrepancies at larger angles for resonant and non-resonant energies are very similar. We conclude that the bending mode resonance $^2\Pi_u$ at 3.8 eV plays no significant role in exciting the Σ_u stretching mode and attribute the discrepancies to the neglect of short-range interactions which interfere destructively with the dominant dipole interaction.

So far, the hot band Π_u (010)→Π_g (011) at 2 meV less energy loss than the fundamental has been neglected. Its ro-vibrational cross sections are also given by (1). From the infrared intensity compilation of Rothman and Young (1981), D_v for the hot band is only 2% larger than for the fundamental. Similarly, the Hönl-London factors for the P and R branches differ from the fundamental values by less than 1%. While the Q branch is formally present for the hot band, its Hönl-London factors are smaller than for the P or R branches by more than two orders of magnitude. Therefore the presence of the hot band in figure 2 can now be easily visualised. The P and R

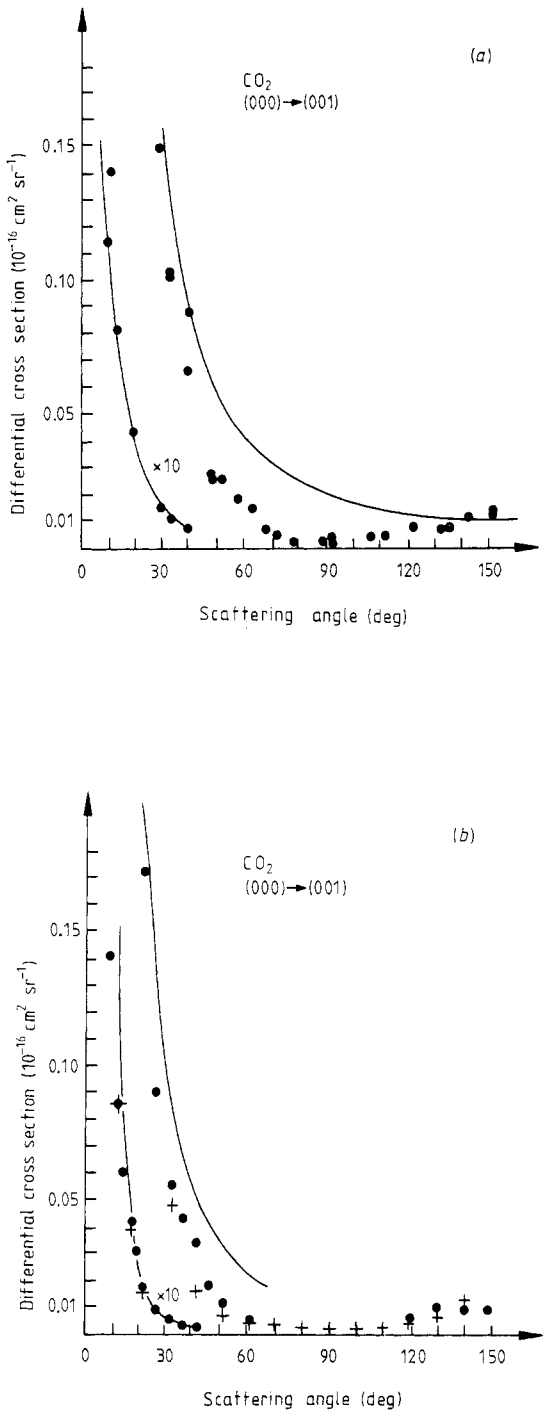

Figure 3. Differential cross sections for excitation of the asymmetric stretch mode. Note the change of scale at $\theta = 30°$. (*a*) Impact energy $E_0 = 2$ eV. • • •, experiment (Danner 1970); ——, Born theory. (*b*) Experiment: • • •, Danner (1970), $E_0 = 3.6$ eV; +++, Register *et al* (1980), $E_0 = 4$ eV. Theory: ——, Born calculation for $E_0 = 3.8$ eV.

branch envelopes are both reduced by 22% and compensated by the hot-band envelopes shifted by 1.5 meV towards lower energy loss. For most scattering angles a slightly better fit of the profile is obtained. For all practical purposes, the deconvoluted DCS with or without hot bands are the same. Therefore hot bands are not discussed in the analyses of other modes.

4.2. The bending mode, Π_u (010)

At 2 eV, the DCS at low resolution has been measured by Danner (figure 4). With the improved measured value for the transition moment $D_2 = 0.0713\ ea_0$ (rather than $0.0589\ ea_0$ used by Danner), the Born theory is in remarkable agreement with his data and our high-resolution vibrational data (5-15°).

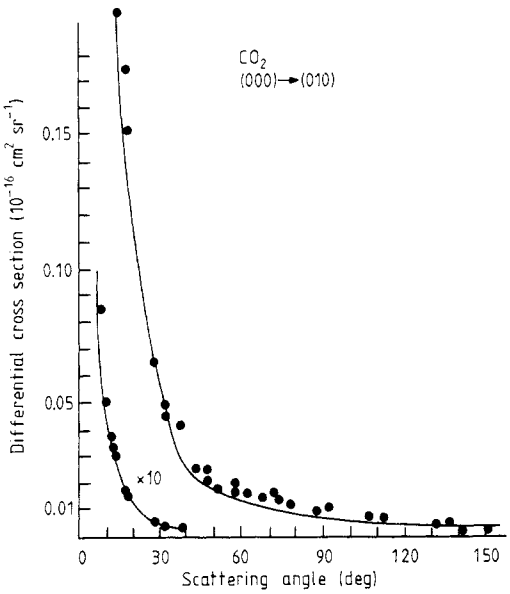

Figure 4. Differential cross section for excitation of the bending mode at $E_0 = 2$ eV. Note the change of scale at $\theta = 30°$. Experiment: • • •, Danner (1970). Theory: ——, Born calculation.

For the $\Sigma_g \rightarrow \Pi_u$ transition, all three branches P, Q, and R are present with their peaks separated by 1 meV. Even with our best resolution of 11 meV, the energy loss profiles still cannot be uniquely unfolded into the rotational branches. Instead we construct branch profiles from theoretical Hönl-London factors and compare their sums with the measured profile for $\theta = 10°$ in figure 5. Not shown are similar data for $\theta = 5$ and 15°. The excellent accord shows that the Born theory given by (1) describes ro-vibrational excitation of the bending mode very well.

The vibrational DCS data at the resonant energy of 3.8 eV are shown as data points in figure 6. Similar results have been obtained by Danner (1970) at 3.6 eV and by Register *et al* (1980) at 4 eV. Assuming only one partial wave in the resonance, theory gives a moderate fit (broken curve) for angles greater than 30°. Even with three partial waves in the resonance theory of Andrick and Read (1971), the fit to the data at 5°

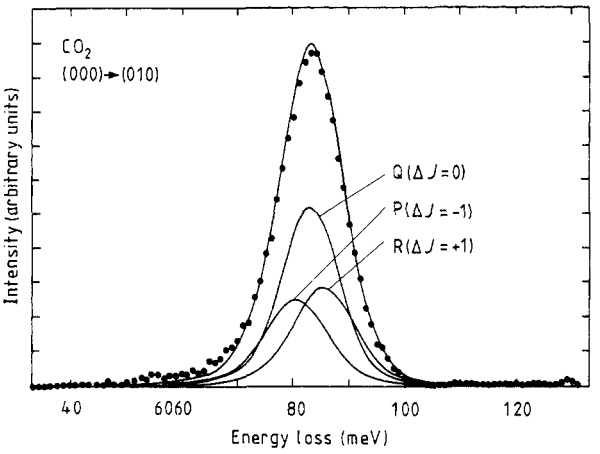

Figure 5. The experimental energy loss profile for excitation of the bending mode at 2 eV impact energy and at $\theta = 10°$. The three calculated rotational branches are shown and their sum is compared with the measured profile.

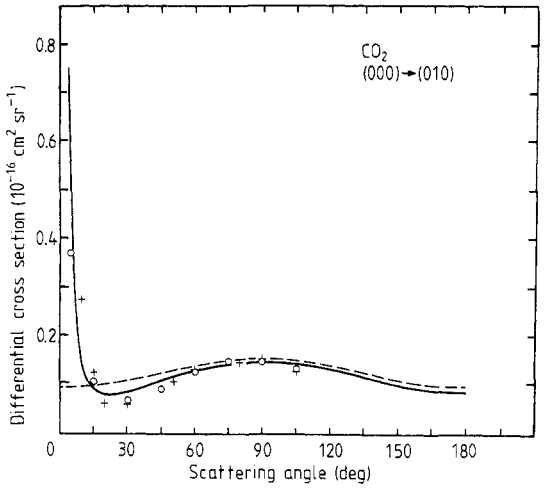

Figure 6. Differential cross section for bending mode excitation at 3.8 eV impact energy. Experiment: +++, Register *et al* (1980); ∘∘∘, present. Theory: – – –, pure resonance, i.e. only joint term of (4); ——, Full (4) with the fitted values of the parameters $\cos\chi = -1$ and $R = 0.524$. The calculation further includes the hot-band transitions.

and 10° was unsatisfactory. In contrast, results of (4) with the free parameters adjusted to $R = 0.524$ and $\cos\chi = -1$ fit the data at all angles within experimental uncertainties. Thus, the dipole interaction which is responsible at all angles when off resonance, still dominates here at low angles. At larger angles the one-partial-wave description of the resonance is adequate, while in between 15 and 30° the short- and long-range interactions interfere destructively.

With the fitted values of R and $\cos\chi$, the rotational DCS can be calculated from (3) and the branch profiles constructed. These are then compared with the measured profiles shown in figure 7. In general, the sum of theoretically constructed branches fit the measured profiles very well, although less so for the two smallest angles. At 5°

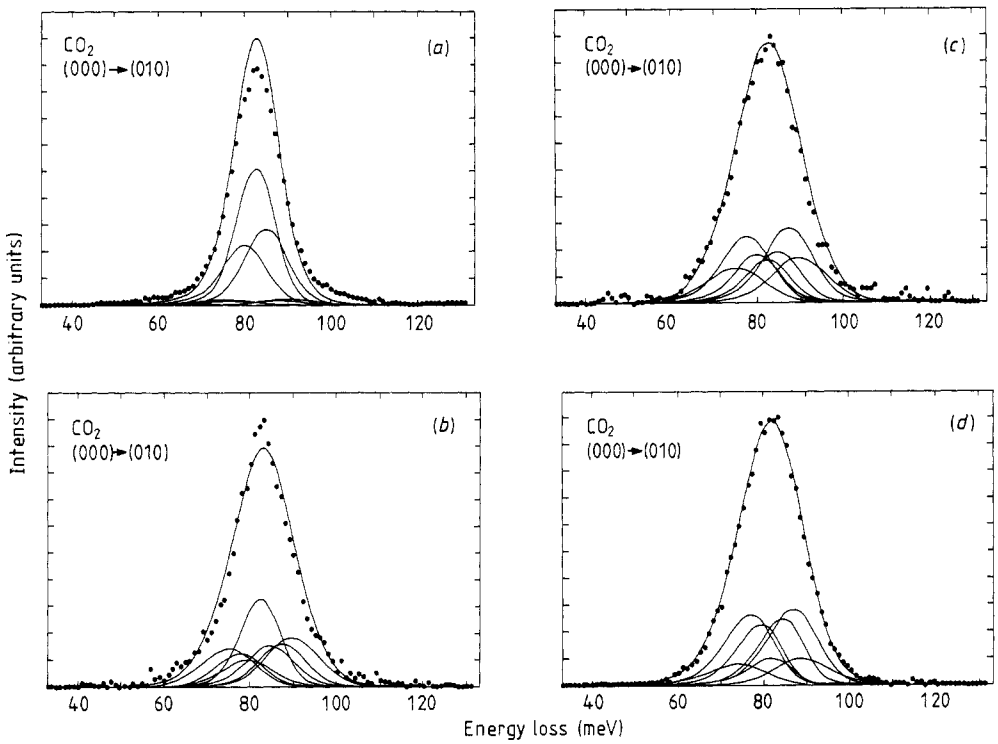

Figure 7. Comparison between measured and calculated line profiles for bending mode excitation in the region of the $^2\Pi_u$ resonance. Impact energy: $E_0 = 3.8$ eV. Scattering angles: (*a*) 5°, (*b*) = 15°, (*c*) 45° and (*d*) 105°. The calculations are based on (3) and include additional (but practically negligible) contributions from hot-band transitions.

(figure 7(*a*)), the profile is almost as narrow as the non-resonant one in figure 5, since the $\Delta j = \pm 2$ and ± 3 branches are barely discernible. By 15° (figure 7(*b*)), all branches are already comparable, so the profile broadens considerably. As the angle increases the contribution of the Q branch decreases, causing a gradual widening of the profile (figure 7(*c*), (*d*)). Explicit angular dependences of the rotational DCS calculated from (3) with $j = 20$ are displayed in figure 8 along with their sum and the measured vibrational cross section. At angles below 15°, the Q and the R branches dominate, while between 45° and 135° the $\Delta j = +3$ branch gives the largest contribution.

4.3. The Raman modes: Fermi diads, $\Sigma_g(\nu_1$ and $\nu_4)$

Earlier lower resolution experiments (Andrick *et al* 1969, Danner 1970) on the excitation of the Raman modes typically measured the sum of both Fermi diads with the energy loss centred at the upper diad (172 meV). In the impact energy range of 1 to 2 eV, the DCS was nearly isotropic and energy independent. These features are confirmed by the present higher resolution data at an impact energy of 2 eV. As can be seen in figures 9(*a*), 9(*b*) and 9(*c*), the measured energy loss profiles peak at 172 meV for all angles. Careful scrutiny of the profiles reveals a low-energy shoulder attributed to the lower diad at 159 meV by unfolding. Further lineshape analysis shows that additional

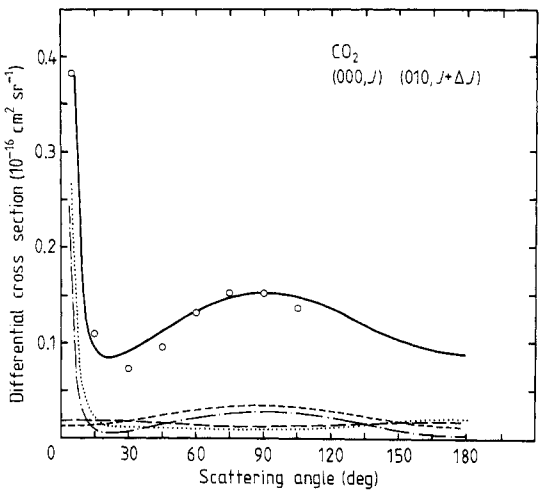

Figure 8. Differential cross sections for excitation of the bending mode and the associated ro-vibrational transitions at 3.8 eV impact energy. Experimental data are represented by circles. Calculated DCS (resulting from (3) with $\cos\chi = -1$ and $R = 0.524$) are shown for these rotational branches: ∘∘∘, $\Delta j = 0$; — · —, $\Delta j = +1$; - - -, $\Delta j = +2$; — —, $\Delta j = +3$; ——, sum ($\Delta j = -3 \cdots +3$).

O and S branches ($\Delta j = \pm 2$) for both vibrational modes are sufficient for a satisfactory fit.

The angular dependences resulting from the unfolding procedure are displayed in figure 10. Considering first the rotationally unresolved cross sections, the upper (figure 10(a)) exceeds the lower diad (figure 10(b)) by an order of magnitude, with both DCS being essentially isotropic. From figure 10(c) it can be seen that the data analysis did not reveal a cross section for the (0 2^2 0) Δ state at 165 meV for larger scattering angles.

Returning to figures 10(a) and 10(b), the ratio of the two Q-branch cross sections is about $0.03/0.0015 = 20$. As the energy loss profiles given in figure 9 have already indicated, this value contrasts sharply with the Raman intensity ratio 1.5 expected from (4). Thus our experiment does not support the view that vibrational excitation of the Raman modes is dominated by the long-range polarisability interaction (Breig and Lin 1965, Itikawa 1971). Instead it suggests that short-range molecular interaction may play a more important role as originally advanced by Wu (1947). On the other hand, the observed sums of the O and S branch cross sections for the two Fermi diads are 0.005 and 0.003×10^{-16} cm^2 sr^{-1}, with the sum of the integrated cross sections being 0.1×10^{-16} cm^2. For pure quadrupole interaction, Born approximation based on the first term of (6) and Q_v given in table 1 results in 0.095×10^{-16} cm^2, in remarkable agreement with the experimental data.

The energy loss profiles at the resonant energy of 3.8 eV are seen in figures 11(a), 11(b) and 11(c) at three different angles. In contrast to the off-resonance profiles (figure 9), their shapes change dramatically with the angle and are considerably broader. Therefore, the ν_1 and the ν_4 DCS are expected to display large angular dependence and to be comparable in size, in contrast to the results at 2 eV. These expectations are shown to be fulfilled in figure 12, which result from unfolding the profiles without resolving the rotational branch structures. The Δ-state cross section here is also found to be negligibly small (see figure 13(c)). While the summed cross section ($\nu_1 + \nu_4$) is

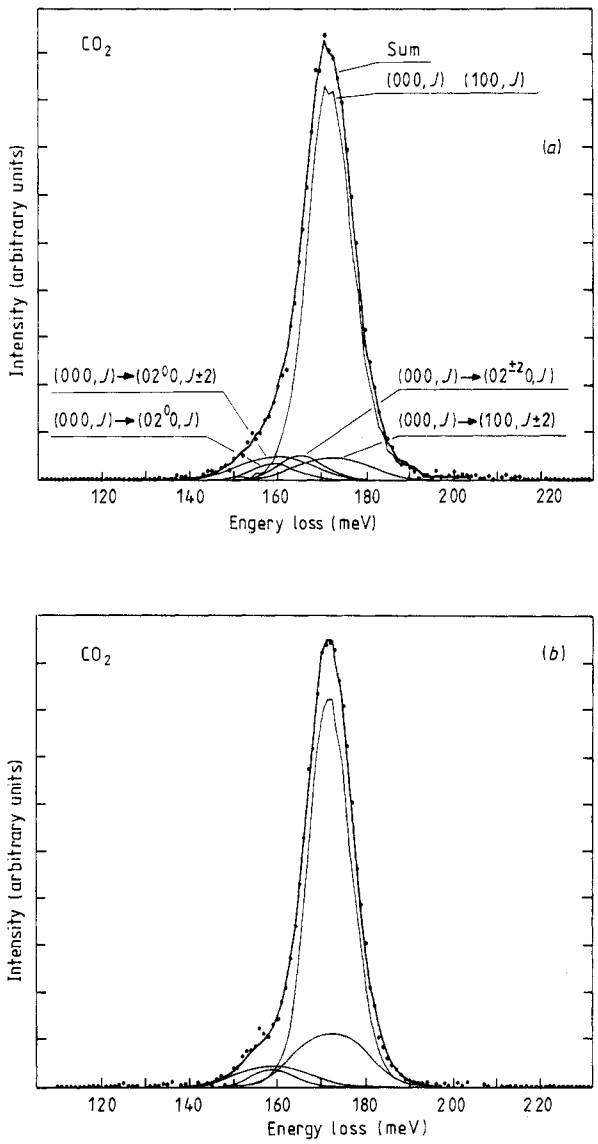

Figure 9.

essentially identical to the 4 eV one of Register *et al* (1980), the individual cross sections display some differences. In particular from $\theta = 80$ to 120°, figure 12 shows that the DCS for ν_1 exceeds that for ν_4 while the opposite is obtained in their data. In any event, our angular dependence of the ν_1 and ν_4 modes (both of Σ_g symmetry) whether separately or summed does not agree well with the one-partial-wave resonance theory (full curve).

By increasing the description of the resonance to three partial waves, Andrick and Read (1971) were able to account for the angular dependence of Danner (1970) which was essentially the same as our summed DCS. However, that a theory with many parameters fitted the data is not necessarily significant. In fact, their theory for the ν_2

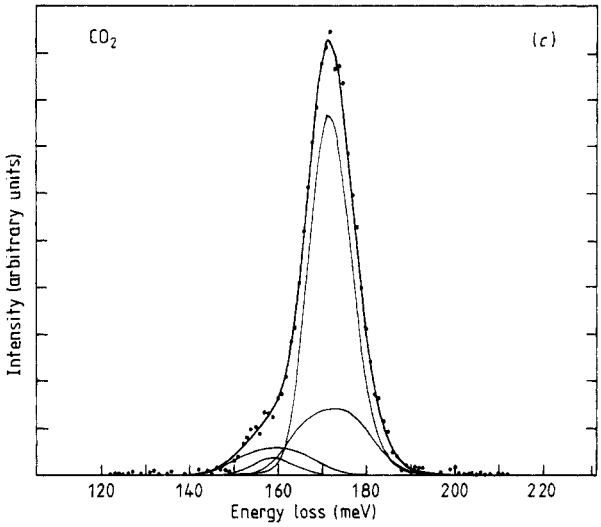

Figure 9. Deconvolution of the rotationally broadened vibrational lines (02^00), (02^20) and (100). The lineshape analysis of the experimental energy loss profile (marked by the data points) includes the O, S and Q branches of each vibrational line. The relative magnitude of these branches is adjusted in a least-squares fit. The sum of all branches, as resulting from the fit, is represented by the line through the data points. The spectra have been taken with 11 meV (FWHM) energy resolution at 2 eV impact energy and scattering angles of (*a*) 15, (*b*) 60 and (*c*) 105°.

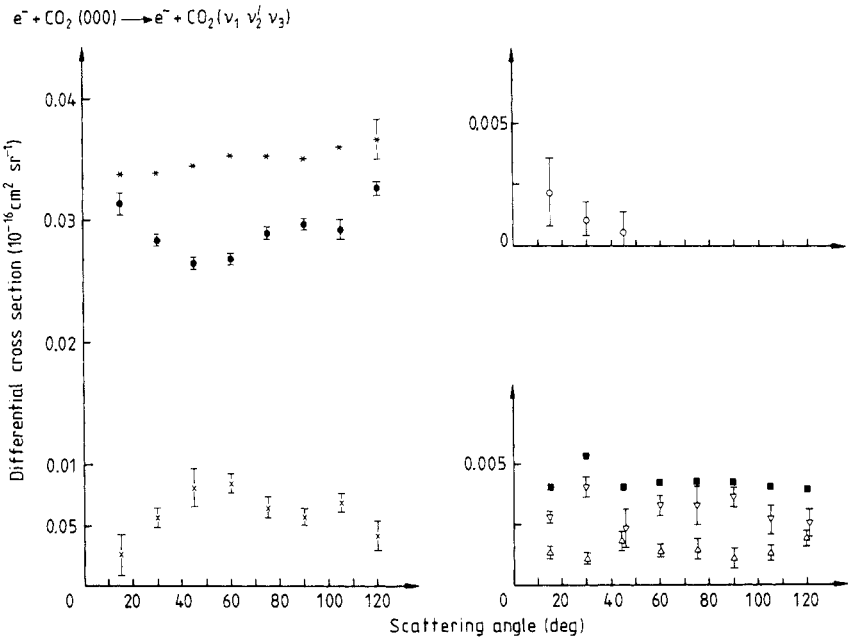

Figure 10. Differential cross sections for excitation of the vibrational modes (02^00), (02^20) and (100) and the associated ro-vibrational transitions as they result from the lineshape analysis of the spectra for 2 eV impact energy. The error bars given in this figure are determined by the numerical uncertainties of the fitting procedure only. *, $(000) \rightarrow (100)$; ●, $(100, J) \rightarrow (100, J)$; ×, $(100, J) \rightarrow (100, J \pm 2)$; ○, $(000) \rightarrow (02^{\pm 2}0, J)$; ■, $(000) \rightarrow (02^00)$; ▽, $(000, J) \rightarrow (02^00, J \pm 2)$; △, $(000, J) \rightarrow (02^00, J)$.

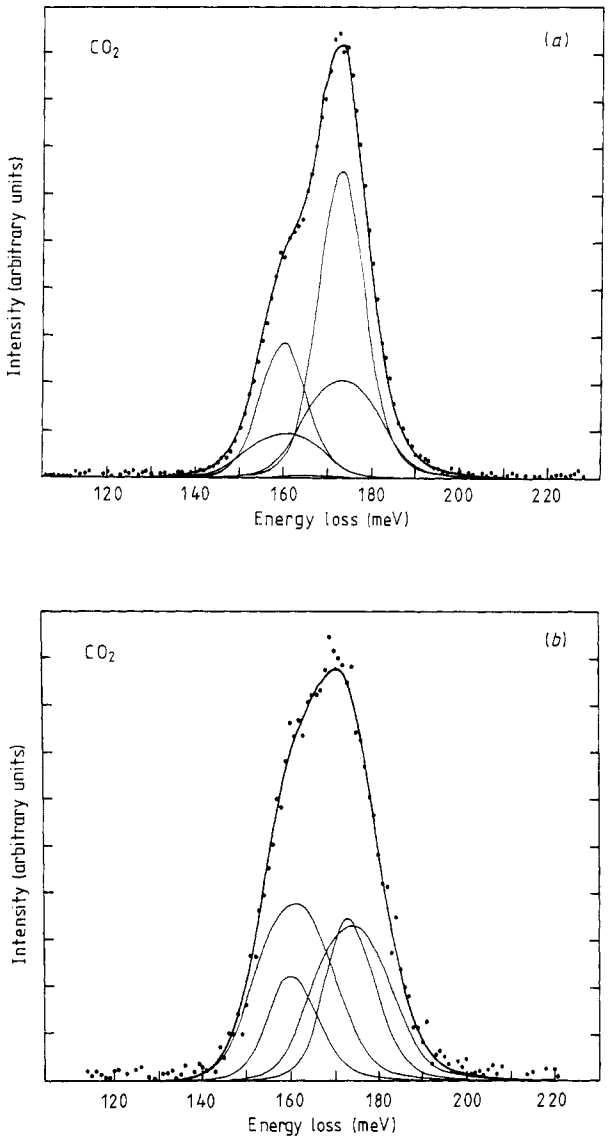

Figure 11.

mode has been refuted by the low angle data (see § 4.2). Further, their assertion of the dominance of the f wave would imply additional rotational branches ($\Delta j = \pm 4$ and ± 6) uncalled for in the fitting of profiles (figure 11). It would also contradict the conclusion of Cadez *et al* (1977) in their study of the excitation of the (n 0 0) progression.

For completeness sake, the rotational branch DCS for the ν_1 and the ν_4 modes obtained by unfolding are shown in figures 13(a) and 13(b), respectively. Note that the O and S branch DCS are considerably flatter than the Q branch DCS as in the cases for N_2 and CO (Jung *et al* 1982). The requisite larger transfer of angular momentum

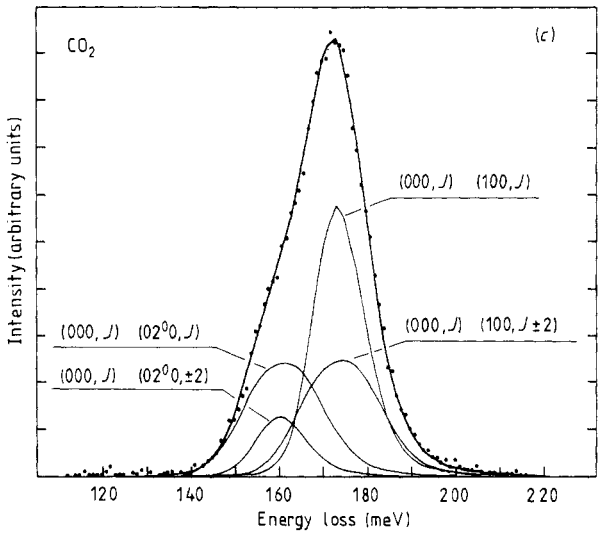

Figure 11. Deconvolution of the rotationally broadened vibrational lines (02^00), (02^20) and (100); lineshape analysis of the experimental energy loss profiles (marked by data points) as described for figure 9. Here the impact energy is 3.8 eV and the scattering angle is (*a*) 15, (*b*) 65 and (*c*) 105°.

may be interpreted as the 'losing of memory of the incident direction' by the electron. Generally these angular dependence data are not explained by any existing theory. It seems that a successful theory has to incorporate the mixing of the (100) and the (020) states, the Π_u resonance, and some direct scattering.

4.4. Integrated cross sections

For the convenience of users and for the comparison of the different modes, we present the integrated cross sections in table 2. The ν_3 parallel transition ($\Sigma \rightarrow \Pi$) is composed of only two rotational branches, each given in the Born approximation at both energies. At 2 eV, the ν_2 cross section is also given by the Born approximation, but it now contains three branches as befits a perpendicular transition ($\Sigma \rightarrow \Pi$). However at 3.8 eV, the $^2\Pi_u$ resonance greatly enhances the ν_2 excitation and results in near-equal contribution of all seven rotational branches allowed for by angular momentum considerations.

The corresponding integrated Raman cross sections are less precisely determined. As mentioned earlier the hot-band problem here is harder to evaluate and without theoretical guidance, angular extrapolation is less reliable. Nevertheless, at 2 eV, the Q branch of the ν_1 mode is an order of magnitude stronger than all other branches (of ν_1 and ν_4). Its value agrees well with the model of Morrison and Lane (1979), while the model of Whitten and Lane (1982) predicts a value too low by more than a factor of two. This latter model is found to give good agreement with the recent low-energy results of Kochem *et al* (1985a), up to about 0.6 eV. Since in this model the 'final-state' wavefunction is determined so that it produces the correct elastic scattering results up to 0.2 eV, one cannot expect that the vibrational excitation cross section will be reliable for energies more than 0.2 eV above the threshold for excitation.

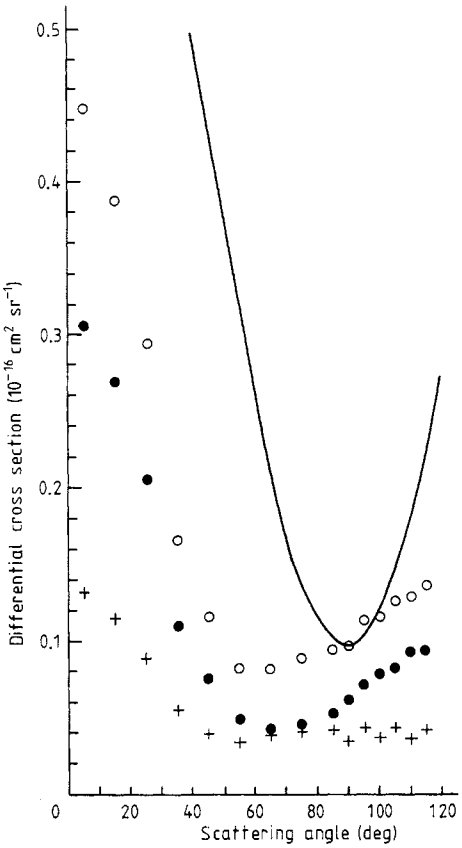

Figure 12. Angular dependences for the excitation cross sections of the vibrational transitions (000)→(02^{0}0): +++, (000)→(100): • • •, without resolving the rotational structure and the sum of these cross sections: ∘∘∘. The experimental data points result from the lineshape analysis of the 3.8 eV spectra. The simple theoretical expression given by (7) does not agree with the data. ○, sum; +, (000)→(02^{0}0); ●, (000)→(100); ——, theory (pπ wave only).

In all theoretical models the Raman cross section drops by a factor of two while measurements (Danner 1970) indicate that it does not depend on energy from 1 to 2 eV. Finally, at 3.8 eV the $^2\Pi_u$ resonance again increases the Raman cross sections with all allowed rotational branches contributing comparably. For all vibrational modes, our integrated cross sections are in very good agreement with those of Danner (1970) which have been evaluated without consideration of hot bands or of theory.

Acknowledgment

This work has been supported by the Deutsche Forschungsgemeinschaft (Sonderforschungsbereich 91).

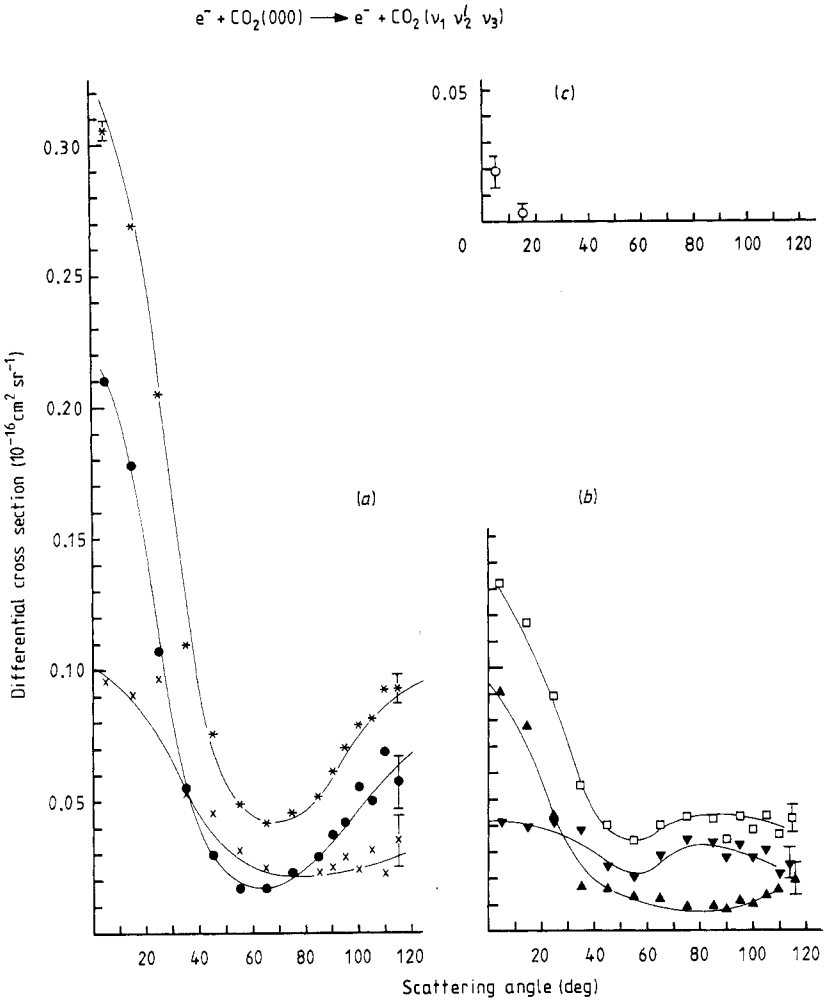

Figure 13. Differential cross sections for excitation of the vibrational modes (02^20), (02^00) and (100) and the associated ro-vibrational transitions as they result from the lineshape analysis of the spectra recorded at 3.8 eV impact energy. *, $(000) \rightarrow (100)$; ●, $(000, J) \rightarrow (100, J)$; ×, $(000, J) \rightarrow (100, J \pm 2)$; □, $(000) \rightarrow (02^00)$; ▲, $(000, J) \rightarrow (02^00, J)$; ▼, $(000, J) \rightarrow (02^00, J \pm 2)$; ○, $(000, J) \rightarrow (02^{\pm 2}0, J)$.

References

Akhmedzhamov R, Atakhodzhaev A K and Bulanin M O 1982 *J. Mol. Struct.* **89** 285-91
Andrick D and Bitsch A 1975 *J. Phys. B: At. Mol. Phys.* **8** 393-410
Andrick D, Danner D and Ehrhardt H 1969 *Phys. Lett.* **29A** 346-7
Andrick D and Read F H 1971 *J. Phys. B: At. Mol. Phys.* **4** 389-96
Breig E L and Lin C C 1965 *J. Chem. Phys.* **43** 3839-45
Cadez I M, Gresteau F, Tronc M and Hall R I 1977 *J. Phys. B: At. Mol. Phys.* **10** 3821-34
Chang E S 1984 *J. Phys. B: At. Mol. Phys.* **17** 3341-51
Chang E S, Antoni Th, Jung K and Ehrhardt H 1984 *Phys. Rev.* A **30** 2086-8
Danner D 1970 *Diplomarbeit* Freiburg, West Germany

Devi V M, Freidovich B, Jones G D and Snyder D G S 1984 *Mol. Phys.* **105** 1-9
Gerjuoy E and Stein D 1955 *Phys. Rev.* **97** 1671-9
Howard-Lock H E and Stoicheff B P 1971 *J. Mol. Spectrosc.* **37** 321-6
Itikawa Y 1971 *Phys. Rev.* A **3** 831-2
Jung K, Antoni Th, Müller R, Kochem K-H and Ehrhardt H 1982 *J. Phys. B: At. Mol. Phys.* **25** 3535-55
Kochem K-H, Sohn W, Hebel N, Jung K and Ehrhardt H 1985a *J. Phys. B: At. Mol. Phys.* **18** 4455-67
Kochem K-H, Sohn W, Jung K, Ehrhardt H and Chang E S 1985b *J. Phys. B: At. Mol. Phys.* **18** 1253-66
Lane N F 1980 *Rev. Mod. Phys.* **52** 29-119
Morrison M A and Lane N F 1977 *Phys. Rev.* A **16** 975-80
—— 1979 *Chem. Phys. Lett.* **66** 527-30
Morrison M A, Lane N F and Collins L A 1977 *Phys. Rev.* A **15** 2186-201
Register D F, Nishimura H and Trajmar S 1980 *J. Phys. B: At. Mol. Phys.* **13** 1651-62
Rothman L S and Young L D G 1981 *J. Quant. Spectrosc. Radiat. Transfer* **25** 505-24
Sohn W, Kochem K H, Jung K, Ehrhardt H and Chang E S 1985 *J. Phys. B: At. Mol. Phys.* **18** 2049-55
Srivastava S, Chutjian A and Trajmar S 1975 *J. Chem. Phys.* **63** 2659-65
Takayanagi K 1966 *Phys. Soc. Japan* **21** 507-14
—— 1984 *Electron-Molecule Collisions* ed I Shimamura and K Takayanagi (New York: Plenum)
Trajmar S and Cartwright D C 1983 *Electron-Molecule Interactions and Their Applications* ed L G Christophorou (New York: Academic)
Whitten B L and Lane NF 1982 *Phys. Rev.* A **26** 3170-6
Wu T Y 1947 *Phys. Rev.* **71** 111-8